ACS Infectious Diseases

pubs.acs.org/journal/aidcbc

Article

Human Cathelicidin Inhibits SARS-CoV-2 Infection: Killing Two Birds with One Stone

Cheng Wang,[#] Shaobo Wang,[#] Daixi Li,[#] Peiqin Chen, Songling Han, Gaomei Zhao, Yin Chen, Jianqi Zhao, Jiachuan Xiong, Jingfei Qiu, Dong-Qing Wei,* Jinghong Zhao,* and Junping Wang*

Cite This: https://doi.org/10.1021/acsinfecdis.1c00096

Read Online

ACCESS | Metrics & More | Article Recommendations | Supporting Information

ABSTRACT: SARS-CoV-2 infection begins with the association of its spike 1 (S1) protein with host angiotensin-converting enzyme-2 (ACE2). Targeting the interaction between S1 and ACE2 is a practical strategy against SARS-CoV-2 infection. Herein, we show encouraging results indicating that human cathelicidin LL37 can simultaneously block viral S1 and cloak ACE2. LL37 binds to the receptor-binding domain (RBD) of S1 with high affinity (11.2 nM) and decreases subsequent recruitment of ACE2. Owing to the RBD blockade, LL37 inhibits SARS-CoV-2 S pseudovirion infection, with a half-maximal inhibitory concentration of 4.74 μg/mL. Interestingly, LL37 also binds to ACE2 with an affinity of 25.5 nM and cloaks the ligand-binding domain (LBD), thereby decreasing S1 adherence and protecting cells against pseudovirion infection *in vitro*. Intranasal administration of LL37 to C57 mice infected with adenovirus expressing human ACE2 either before or after pseudovirion invasion decreased lung infection. The study identified a versatile antimicrobial peptide in humans as an inhibitor of SARS-CoV-2 attachment using dual mechanisms, thus providing a potential candidate for coronavirus disease 2019 (COVID-19) prevention and treatment.

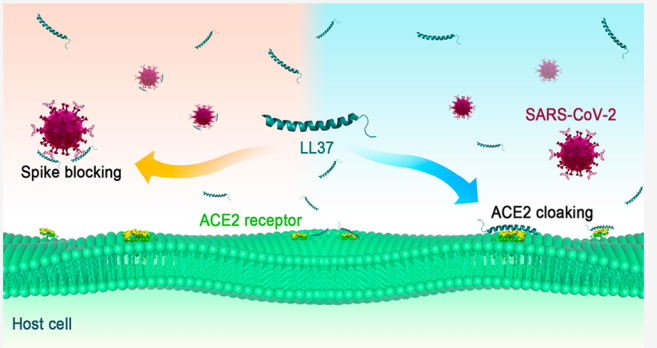

KEYWORDS: *cathelicidin, SARS-CoV-2, spike, receptor binding domain, angiotensin-converting enzyme-2*

Coronavirus disease 2019 (COVID-19) resulting from severe acute respiratory syndrome coronavirus 2 (SARS-CoV-2) infection is a serious threat to human health and to date has infected over 120 000 000 people and caused more than 2 000 000 deaths.[1] SARS-CoV-2 is an enveloped, positive-sense RNA virus with a genome encoding the spike (S) protein, envelope protein, membrane protein, and nucleoprotein. The S protein, composed of the S1 and S2 subunits, exists as a trimer in solution.[2] SARS-CoV-2 invades host cells, initiated by the adherence of S1 to the membrane via recognition of critical receptor angiotensin-converting enzyme-2 (ACE2),[3] a negative regulator of the renin-angiotensin system. With the proteolysis of transmembrane protease serine-2 (TMPRSS2),[4] S1 dissociates and S2 mediates viral entry into the cytoplasm.[5]

Interferons (IFNs) and antimicrobial peptides (AMPs), effectors of the host innate immune system, represent the first line of defense against SARS-CoV-2. Pneumonia occurs when SARS-CoV-2 runs the blockade of innate immunity and reaches the pulmonary alveoli. The subsequent strong adaptive immune response results in a cytokine storm, acute respiratory disease syndrome (ARDS), and other severe complications.[6] Human innate immunity can eliminate SARS-CoV-2 but is impaired in COVID-19 patients,[7] as manifested by the low levels of type I and III IFNs.[8,9] To correct the imbalanced host response to SARS-CoV-2, the administration of type I IFN is proposed as a therapeutic strategy for COVID-19 in the early stage of infection.[10] In addition, AMPs are also altered to varying degrees after SARS-CoV-2 infection,[8] although less is known about the role of the changed AMPs in COVID-19 pathogenesis.

AMPs are extensively present in flora and fauna and have the general characteristics of electropositive charge, amphipathy, and a low molecular weight (typically 12 to 50 amino acids). AMPs are divided on the basis of the spatial conformation into four major groups: β-stranded peptides, α-helices, extended helices, and peptides with loop structures.[11] Defensins and cathelicidins are two important groups of mammalian AMPs. Human defensins (HDs) are β-stranded peptides with evolutionarily conserved elements in the sequence.[12] We recently discovered that HD5, an intestinal AMP whose

Special Issue: Antiviral Therapeutics

Received: February 23, 2021

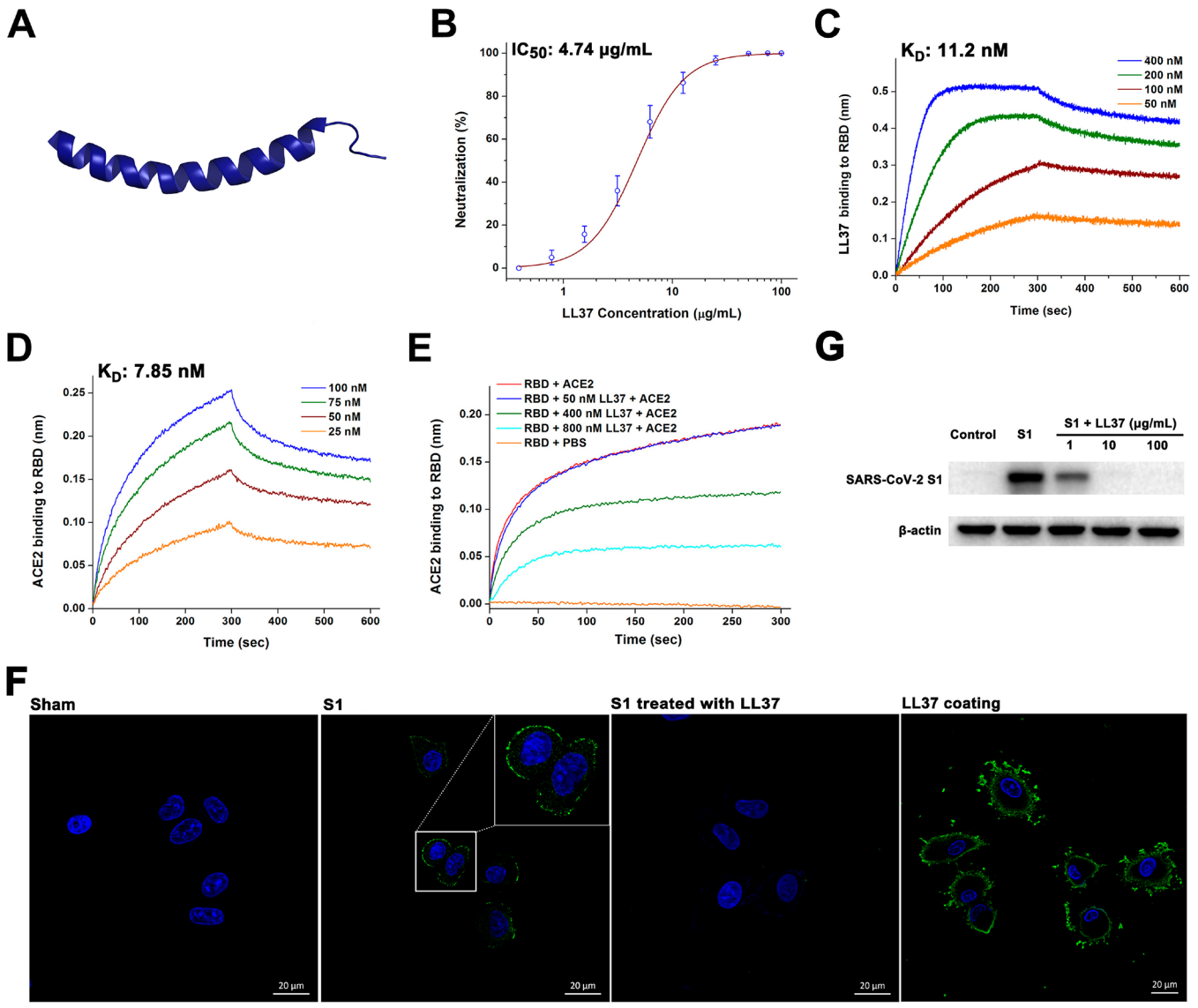

Figure 1. LL37 suppresses S1 associating with ACE2 by blocking RBD. (A) Ribbon structure of LL37 (PDB: 2K6O) in lipid micelles. (B) IC_{50} determination. Results shown as the mean ± standard deviation (SD) were processed by a nonlinear curve fit. (C) Binding kinetics for LL37 and RBD. (D) Binding kinetics for ACE2 and RBD. (E) BLI-based RBD blocking assay. (F) Immunofluorescence microscopy revealing the inhibition of LL37 on S1 (Green) adhering to A549 cells and the coating of LL37 (Green) on the cell membrane. The region of interest in the S1-treated group is magnified in the embedding graph. The scale bar indicates 20 μm. (G) Protein bands of S1 pretreated with increasing concentrations of LL37 binding to A549 cells. β-actin is the reference.

expression is increased after viral infection,[13] inhibited SARS-CoV-2 invasion by cloaking ACE2.[14] The LL37 peptide is derived from the hCAP-18 protein, which is encoded by the *CAMP* gene. LL37 belongs to the α-helix group (Figure 1A) and is the only member of the human cathelicidin family discovered to date.[15] The human respiratory tract epithelium produces LL37 to antagonize invading microbes.[16] Because of an increase in *CAMP* gene expression in the lungs of COVID-19 patients compared with uninfected controls,[8] we speculated that similar to HD5, LL37 might play a role in host defense against SARS-CoV-2 infection.

Herein, we evaluated the antiviral properties of LL37 against SARS-CoV-2 *in vitro* and *in vivo* using S pseudovirions. The antiviral mechanism of LL37 was investigated by biolayer interference (BLI) and molecular dynamic simulation (MDS). Our study sheds light on an innate immune element in humans functioning as an inhibitor of SARS-CoV-2 attachment, offering possibilities for COVID-19 prevention and treatment.

RESULTS AND DISCUSSION

LL37 Binds to the Receptor-Binding Domain (RBD) and Inhibits S1 Recruitment. To evaluate the effect of LL37 on viral invasion, we employed SARS-CoV-2 S pseudovirions equipped with a luciferase reporter system to infect human embryonic kidney-239T cells with a high expression of ACE2 (HEK-293T-hACE2 cells)[17] in the presence of increasing concentrations of synthetic LL37 (Figure S1). LL37 suppressed S pseudovirion infection in a dose-dependent manner with a half-maximal inhibitory concentration (IC_{50}) of 4.74 μg/mL (1.05 μM, Figure 1B), which was lower than those of ACE2-derived peptide inhibitors for suppressing S pseudovirion infection.[18] However, LL37 was less efficient than neutralizing antibodies and recombinant ACE2 fused with

https://doi.org/10.1021/acsinfecdis.1c00096
ACS Infect. Dis. XXXX, XXX, XXX−XXX

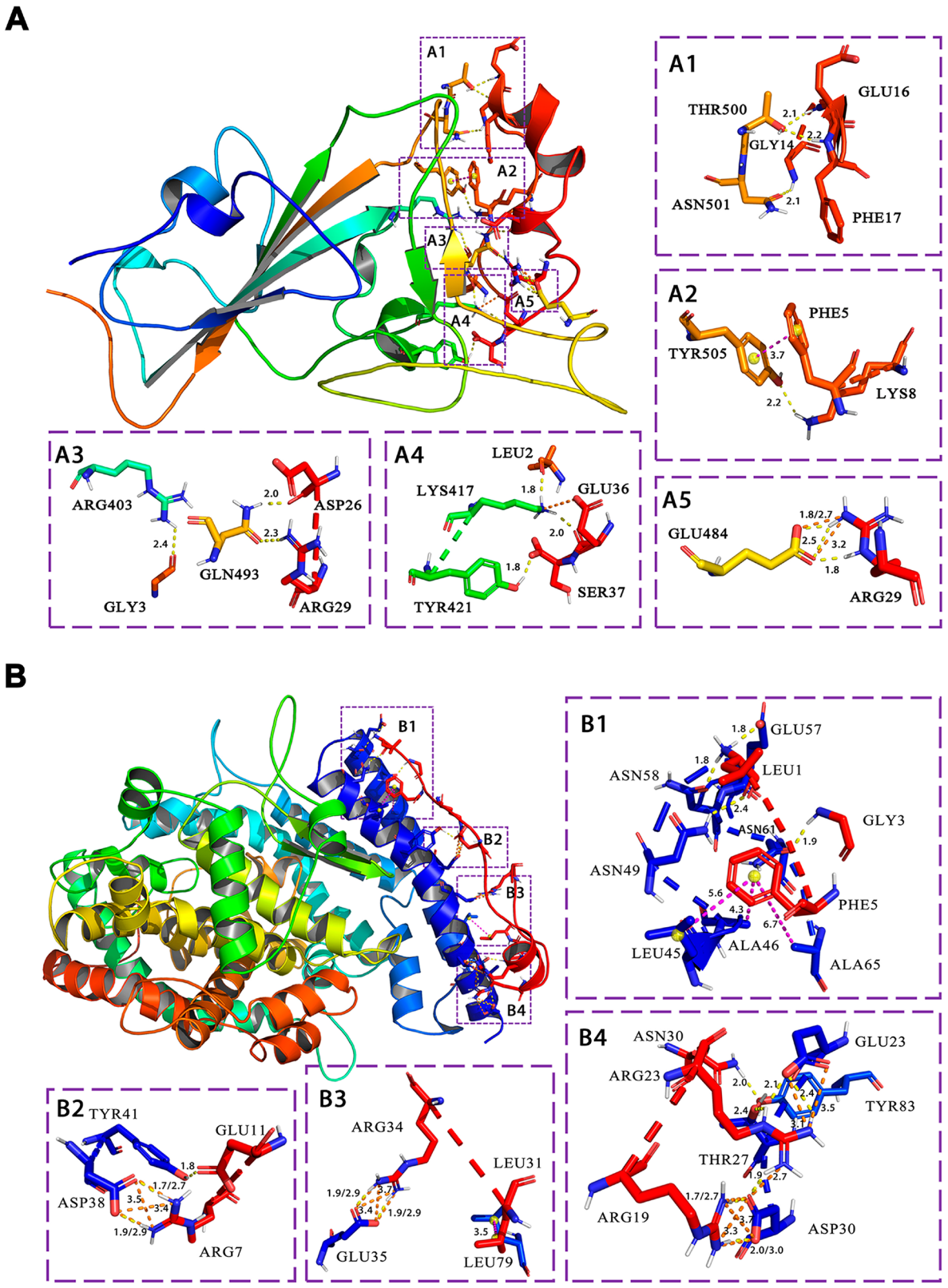

Figure 2. Complex structures of LL37 with SARS-CoV-2 RBD (A) and ACE2 (B). RBD and ACE2 (PDB: 6M0J) are shown in the ribbon structure. LL37 is shown in the red ribbon on the right. Salt bridges, hydrogen bonds, and hydrophobic interactions are shown in orange, yellow, and purple, respectively.

the Fc region of human immunoglobulin G1 (IgG1) in blocking SARS-CoV-2 S pseudovirion infection.[19,20]

S1, which contains an RBD, is the ligand of ACE2. To gain insight into the antiviral mechanism, we used BLI to analyze the recruitment of LL37 to the RBD. The binding affinity of LL37 for biotinylated RBD immobilized on streptavidin (SA) biosensors was 11.2 nM (Figure 1C), comparable to that of ACE2 for the RBD (7.85 nM, Figure 1D). To assess the

https://doi.org/10.1021/acsinfecdis.1c00096
ACS Infect. Dis. XXXX, XXX, XXX−XXX

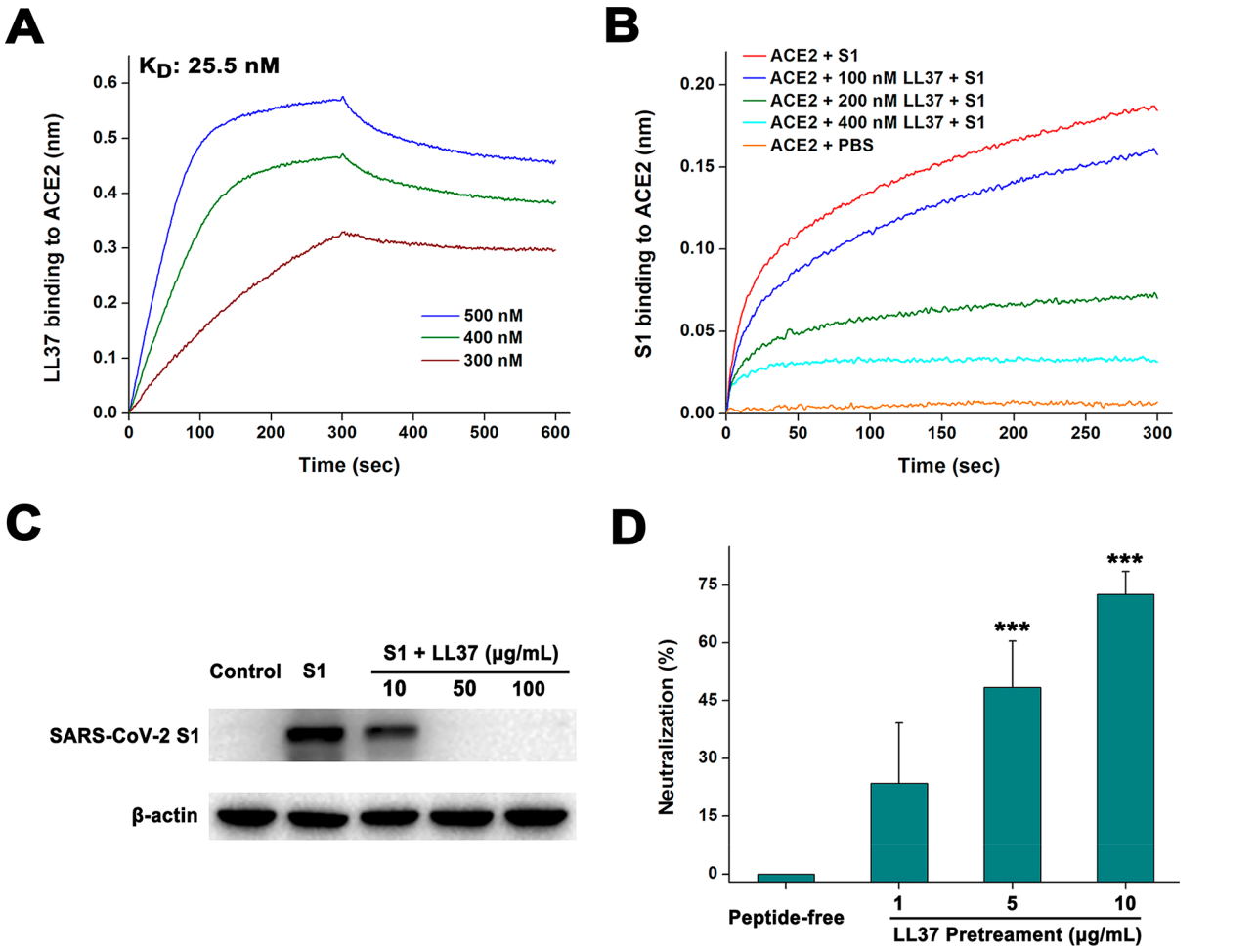

Figure 3. LL37 attenuates S1 binding to cells by cloaking ACE2. (A) Binding kinetics for LL37 and ACE2. (B) BLI-based ACE2 blocking assay. (C) Protein bands of S1 binding to A549 cells pretreated with increasing concentrations of LL37. β-actin is the reference. (D) Pseudovirion neutralization assay. Results are shown as the mean ± SD. Compared with the peptide-free group, the cells pretreated with 5 and 10 μg/mL LL37 were less sensitive to SARS-CoV-2 S pseudovirion infection. ***, $P < 0.001$.

influence of the LL37 coating on ACE2 recruitment via the RBD, a blocking experiment was carried out by monitoring the binding of ACE2 to the RBD coated with increasing concentrations of LL37. As shown in Figure 1E, LL37 dose-dependently decreased the signals corresponding to ACE2 binding to the RBD. A cell experiment in which human pulmonary epithelial A549 cells were exposed to 10 μg/mL S1 in the presence and absence of LL37 was then performed. Confocal microscopy revealed that S1 adhered predominantly to the cell surface (Figure 1F). When S1 was pretreated with 20 μg/mL LL37 at 37 °C for 15 min, its recruitment was markedly reduced. Western blot analysis supported the finding that LL37 dose-dependently decreased the adherence of S1 to cells (Figure 1G). The inhibitory effect of LL37 on S1 adherence was also observed for human renal tubular epithelial HK-2 cells (Figure S2), which express an abundance of ACE2 and are susceptible to SARS-CoV-2 infection.[21,22]

LL37 has an N-terminal region (residues 1−13) that is responsible for its proteolysis resistance, a core antimicrobial domain (residues 18−29), and a C-terminal sequence (residues 32−37) that participates in tetramer formation.[23] To identify the active region of LL37 mediating S1 suppression, we generated five truncated derivatives (Figure S1). Circular dichroism (CD) scanning showed that similar to wild-type LL37, the mutants excluding the C-terminal coil (NL8) displayed random coils and α-helical structures in ultrapure water and sodium dodecyl sulfonate micelles, respectively (Figure S3A). However, Western blot analysis revealed that sequence truncation suppressed the inhibitory effect of LL37 (Figure S3B), which suggests that LL37 blocks S1 adherence in a manner dependent on the primary structure, consistent with its structure-dependent antiviral action against dengue virus.[24]

The SARS-CoV-2 RBD binds to ACE2 with 18 contacting residues (i.e., LYS417, GLY446, TYR449, TYR453, LEU455, PHE456, ALA475, PHE486, ASN487, TYR489, GLN493, TYR495, GLY496, GLN498, THR500, ASN501, GLY502, and TYR505).[25] Neutralizing antibody P2B-2F6 binds to the RBD and captures 12 residues, including 2 contacting residues, GLY446 and TYR449, which precludes ACE2 receptor engagement.[26] Additionally, miniprotein inhibitor LCB3 binds to the RBD with picomolar affinity via 38 binding sites, 14 of which overlap with the contacting residues of the RBD involved in ACE2.[27] Our MDS data showed that LL37 formed 3 salt bridges, 13 hydrogen bonds, and a pair of hydrophobic interaction with the RBD (Table S1). Driven by these intermolecular interactions, LL37 bound to eight residues of the RBD within a range of 5 Å, including five

https://doi.org/10.1021/acsinfecdis.1c00096
ACS Infect. Dis. XXXX, XXX, XXX−XXX

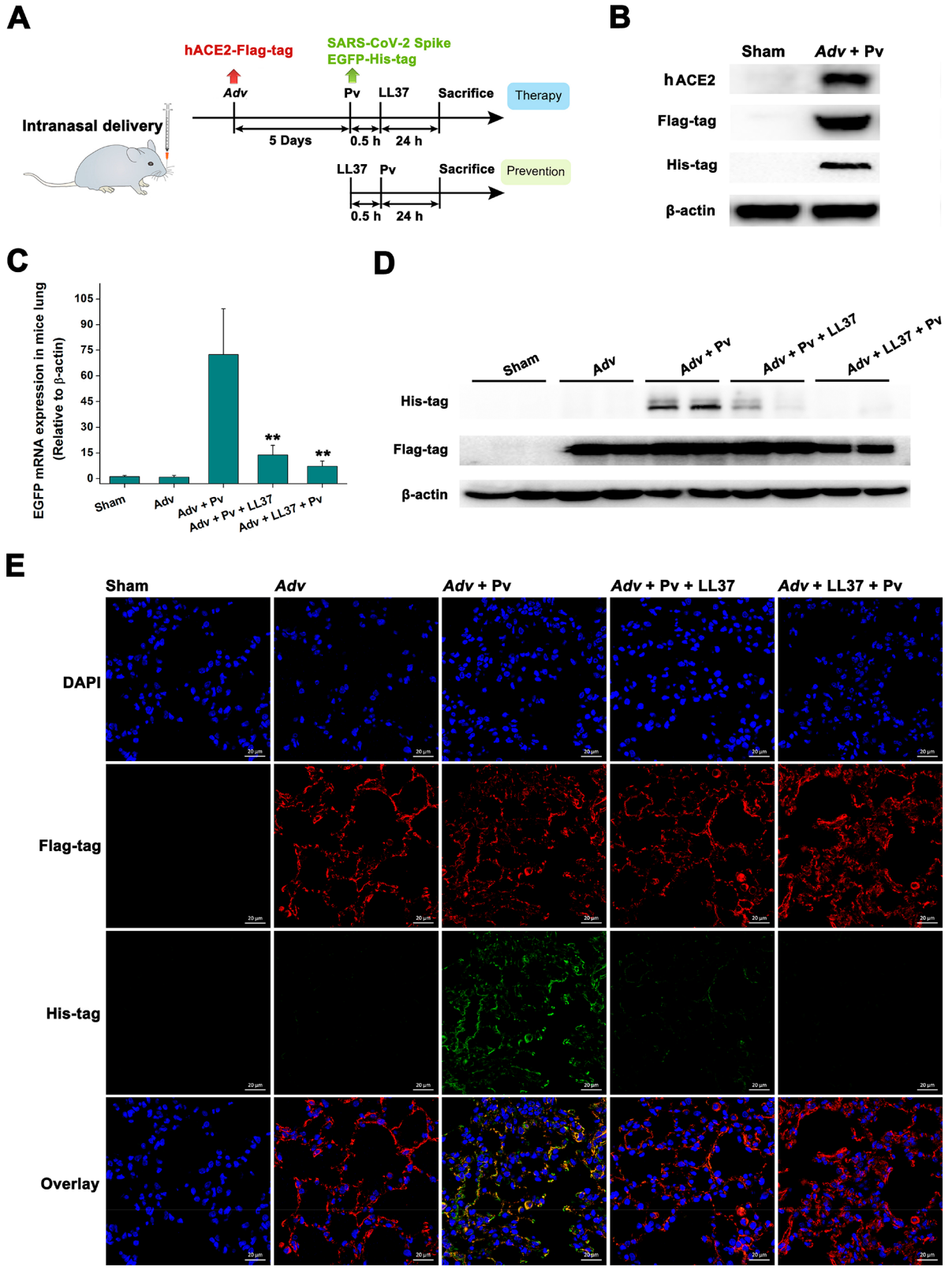

Figure 4. LL37 treatment inhibits pseudovirion infection in mouse lungs. (A) Diagrammatic drawing depicting the pseudovirion-based mouse infection model. Adenovirus, *Adv*; pseudovirion, Pv. (B) Protein bands of ACE2, Flag-tag, and His-tag in Lewis cells infected by the adenoviruses and pseudovirions. β-actin is the reference. In the sham group, the cells were treated with sterile PBS. (C) EGFP mRNA expression relative to β-actin. Results are shown as the mean ± SD **, $P < 0.01$, compared to the sham group in which mice were treated with saline solution. (D) Protein bands of Flag-tag and His-tag in mouse lungs. β-Actin is the reference. (E) Immunofluorescence microscopy revealing the inhibition of LL37 on pseudovirion infection *in vivo*. The scale bar is 20 μm.

https://doi.org/10.1021/acsinfecdis.1c00096
ACS Infect. Dis. XXXX, XXX, XXX−XXX

contacting residues: LYS417, GLN493, THR500, ASN501, and TYR505 (Figure 2A). These findings helped to explain the mechanism by which LL37 blocks RBD binding.

LL37 Cloaks ACE2 and Inhibits Pseudovirion Infection *In Vitro*. LL37 is constitutively expressed *in vivo* and may capture ACE2 before the virus reaches the alveolar epithelial cells. Confocal microscopy indicated the feasibility of this mechanism, as LL37 was localized primarily on the surface of A549 cells (Figure 1F), consistent with the location of HD5 on enterocytes.[14] BLI showed that LL37 bound to ACE2 with an affinity of 25.5 nM (Figure 3A), approximately 3-fold lower than that of HD5 binding to ACE2.[14] To assess the influence of the LL37 coating on the interaction of ACE2 with S1, a BLI-based blocking experiment was conducted. As shown in Figure 3B, LL37 decreased the amount of S1 binding to ACE2, consistent with the Western blot results (Figure 3C). Cell experiments with pseudovirions showed that the pretreatment of A549 (Figure 3D) and HEK-293T-hACE2 (Figure S4) cells with LL37 decreased the viral infection in a dose-dependent manner, thus demonstrating the protective effect of LL37 on sensitive cells by cloaking ACE2.

ACE2 binds to the SARS-CoV-2 RBD at nanomolar affinity with 20 contacting residues (i.e., GLN24, THR27, PHE28, ASP30, LYS31, HIS34, GLU35, GLU37, ASP38, TYR41, GLN42, LEU45, MET82, TYR83, ASN330, LYS353, GLY354, ASP355, ARG357, and ARG393).[25] TYR41 is recognized as a critical residue for the interaction of ACE2 with the RBD.[28] Furthermore, the cloaking of ASP30, LYS31, and TYR83 contributed to the protective effect of HD5 against SARS-CoV-2 attachment to host cells.[14] MDS indicated that LL37 formed 15 salt bridges, 16 hydrogen bonds, and 4 pairs of hydrophobic interactions with the ligand-binding domain (LBD) of ACE2 (Table S2). LL37 bound to 12 residues of the LBD within a range of 5 Å, including ASP30, ASP38, TYR41, and TYR83 (Figure 2B). The blockade of these contacting residues by LL37 might attenuate SARS-CoV-2 S1 binding to ACE2.

Virus propagation depends on living cells via a general lifecycle comprising attachment, entry, replication, assembly, and release.[29] On the basis of the inhibitory mechanism, antiviral agents are divided into two groups: virus-targeting antivirals (VTAs) and host-targeting antivirals (HTAs).[30] HDs act simultaneously as VTAs and HTAs,[31] as exemplified by the binding of human β defensin 3 to viral glycoprotein B and host heparan sulfate, thereby inhibiting herpes simplex virus attachment.[32] In the current study, we found that LL37 suppressed SARS-CoV-2 attachment by blocking viral S attachment and cloaking the host LBD, thus acting as both a VTA and a HTA, indicating the versatility of human AMPs in the innate antiviral defense. Since the outbreak of COVID-19, ample research has been performed to develop efficient inhibitors for SARS-CoV-2 attachment. Most studies have focused on the S protein and have discovered promising antagonists, including neutralizing antibodies and *de novo* designed peptides.[26,27] Additionally, ACE2 cloakers are promising candidates for suppressing viral invasion.[14,33] LL37 integrates the modes of action of ligand blockers and receptor cloakers and is, to our knowledge, the first inhibitor capable of hindering SARS-CoV-2 adherence to target cells via a dual mechanism.

LL37 Suppresses Pseudovirion Infection *In Vivo*. Because SARS-CoV-2 generally enters the human body through the respiratory pathway, topical application of inhibitors to the nose and lung is instrumental for curbing viral infection.[27] LL37 is a natural product with the advantage of low immunogenicity compared with *de novo* designed inhibitors. Additionally, compared to neutralizing antibodies, LL37 is easier to prepare and more suitable for direct delivery into the respiratory system by intranasal administration and aerosolization.[27,34] Inspired by the observation that the *in vivo* potencies of monoclonal antibodies and vaccines against Ebola virus and Lassa virus could be evaluated using pseudovirions outside of BSL-4 laboratories,[35,36] we established a pseudovirion-based mouse pulmonary infection model to assess the inhibitory effect of LL37 on SARS-CoV-2 *in vivo*. Adenoviruses expressing Flag-tagged ACE2, SARS-CoV-2 S pseudovirions expressing His-tagged enhanced green fluorescent protein (EGFP), and LL37 were intranasally administered to mice as depicted in Figure 4A. Mouse Lewis cells infected with the adenoviruses produced ACE2-Flag, resulting in susceptibility to pseudovirion infection (Figure 4B).

We evaluated pseudovirion infection by detecting EGFP and the His tag in lung samples. Either therapeutic or preventive treatment with LL37 significantly decreased pseudovirion infection, as revealed by the quantitative real-time polymerase chain reaction (q-PCR) used to detect EGFP mRNA expression in mouse lungs (Figure 4C). No obvious difference was observed between the therapy and prevention groups. The suppressive effect of LL37 on pseudovirion infection was further confirmed by Western blot analysis (Figure 4D) and immunofluorescence (Figure 4E). Notably, because a pseudovirion cannot replicate in cells as an authentic virus does, these findings cannot accurately reflect the antiviral effects of LL37 against SARS-CoV-2 infection *in vivo*. However, SARS-CoV-2 S pseudovirions are biologically safe and instrumental for investigating attachment inhibitors. The antiviral effects of attachment inhibitors, such as neutralizing antibodies,[26] ACE2-derived peptides,[18] and decoy nanoparticles,[37] against S pseudovirions and live SARS-CoV-2 are consistent. Accordingly, our data indicated that LL37 is a potential prophylactic and therapeutic drug for COVID-19 as a viral attachment inhibitor. LL37 has broad-spectrum antibacterial and antifungal activities.[38] Because a coinfection of bacteria and fungi occurs in COVID-19 patients,[39] LL37 treatment may simultaneously suppress SARS-CoV-2 invasion and prevent infection by respiratory pathogens. Furthermore, LL37 alleviates endotoxin-induced inflammation,[40] activates type I IFN,[41] inhibits neutrophil infiltration, and lowers the production of proinflammatory cytokines in acute lung injury,[42] which may also be beneficial for mitigating the cytokine storm after SARS-CoV-2 infection.

LL37 is stored as a precursor in the granules of epithelial cells and phagocytic cells that are in direct contact with external stimuli.[38] When infection activates Toll-like receptors (TLRs) or alters the cytokine milieu,[43,44] these cells degranulate and release the inactive precursor, which is further processed by proteases to produce LL37.[45] Because of the vitamin D response element (VDRE) sequence in the *CAMP* gene promoter, vitamin D receptor (VDR) activation is a conceivable approach to increasing the production of LL37.[46] VDR agonist 1,25-dihydroxyvitamin D3, the active form of vitamin D, has been identified as an enhancer of LL37 expression.[46] Supplementation with vitamin D is thus considered to be a useful approach to suppressing SARS-CoV-2 infection.[47] Because diet and UV-B light exposure are the main sources of vitamin D in humans, a diet rich in vitamin

https://doi.org/10.1021/acsinfecdis.1c00096
ACS Infect. Dis. XXXX, XXX, XXX−XXX

D and UV-B treatment may be helpful for defending against viral invasion. Moreover, TLR agonists and phenylbutyrate upregulate LL37 production through a vitamin D-dependent pathway.[43,48] Separate from the direct delivery of LL37 to the focus of infection, the application of these inducers to elevate endogenous LL37 may help to curb the SARS-CoV-2 infection.

CONCLUSIONS

Mammalian AMPs have evolved to antagonize invading microbes. In the present study, we discovered that LL37, an endogenous versatile AMP in humans, may be a potential SARS-CoV-2 attachment inhibitor. LL37 bound to the SARS-CoV-2 RBD, resulting in the competitive inhibition of ACE2 recruitment. Additionally, LL37 was bound to ACE2 and blocked the LBD, which decreased the adherence of S1, a crucial element mediating the attachment of SARS-CoV-2 to sensitive cells. LL37 integrated the modes of action of viral ligand blockers and host receptor cloakers, acting simultaneously as both a VTA and a HTA. Cell and mouse experiments revealed that LL37 suppressed SARS-CoV-2 S pseudovirion infection *in vitro* and *in vivo*. Hence, the direct administration of LL37 or an increase in the expression of endogenous LL37 by host-directed therapy[49] may be instrumental in COVID-19 prevention and treatment.

METHODS

Peptide Synthesis. LL37 and its derivatives were chemically synthesized by Guoping Pharmaceutical Company (Hefei, Anhui, China). The purities and molecular masses of the peptides were determined by high-performance liquid chromatography and mass spectrometry, respectively; data are provided in Figure S1.

***In Vitro* Pseudovirion Infection Assay.** HEK-293T-hACE2 cells obtained from Prof. Ye[50] and A549 cells purchased from the Cell Bank of the Chinese Academy of Sciences (CAS, Shanghai, China) were cultured in Dulbecco's modified Eagle's medium (DMEM, Gibco, Thermo Fisher Scientific, Shanghai, China) containing 10% fetal bovine serum (FBS, Gibco). Cells were seeded into a 96-well plate at a density of 5×10^3 cells/well and cultured overnight. To determine IC_{50}, SARS-CoV-2 S pseudovirions expressing a dual-luciferase reporter (1×10^6 TU, Tsingke Biotechnology, Beijing, China) were pretreated with increasing concentrations of LL37 (100, 75, 50, 25, 12.5, 6.25, 3.13, 1.56, 0.78, and 0.39 μg/mL) at 37 °C for 15 min. After three washes with sterile PBS, HEK-293T-hACE2 cells were coincubated with pseudovirions at 37 °C for 12 h. The cells were further cultured for 48 h in DMEM containing 10% FBS after the removal of pseudovirions. To evaluate the effect of ACE2 cloaking on pseudovirion invasion, A549 and HEK-293T-hACE2 cells were preincubated with LL37 (1, 5, and 10 μg/mL) at 37 °C for 24 h and were then exposed to pseudovirions for 48 h. Luciferase activity was measured using a dual-luciferase reporter assay system (E1910, Promega, Beijing, China). Experiments were conducted in triplicate and repeated twice.

BLI. The binding of LL37 and human ACE2 (10108-H02H, Sino Biological, Beijing, China) to the RBD (40592-V08B-B, Sino Biological) and the binding of LL37 and S1 (40591-V08H, Sino Biological) to ACE2 (10108-H08H-B, Sino Biological) were measured using BLI (Octet Red 96, Sartorius, Göttingen, GER). The RBD and ACE2 were immobilized on SA biosensors at 15 μg/mL. Association and disassociation, 300 s for each, were conducted in PBS at a shaking speed of 1000 rpm. The data were processed using ForteBio Data Analysis 7.0 software. The equilibrium dissociation constant (K_D) was obtained with a 1:1 fitting model. In the blocking assay, immobilized RBD and ACE2 were initially preincubated with LL37 for 300 s at 30 °C. Then, the signals corresponding to the binding of 150 nM S1 to ACE2 and 70 nM ACE2 to the RBD were recorded for another 300 s.

Immunofluorescence Microscopy. A549 cells cultured in DMEM containing 10% FBS were seeded on sterile glass slides in a 12-well plate at a density of 2×10^5 cells/well. After three washes with sterile PBS, the cells were incubated with 10 μg/mL S1 pretreated with 20 μg/mL LL37 at 37 °C for 15 min. Coincubation was continued at 37 °C for 1 h. Normal rabbit IgG (A7016, Beyotime, Shanghai, China, 1:200), an anti-S rabbit polyclonal primary antibody (40591-T62, Sino Biological, 1:200), and a goat antirabbit secondary antibody (Alexa Fluor 488, Invitrogen, Thermo Fisher Scientific) were employed in stain S1. The coating of LL37 on A549 cells was analyzed by incubating 20 μg/mL biotin-labeled LL37 (LL37-004B, Chinese Peptide Company, Hangzhou, China) with cells at 37 °C for 1 h. A primary antibiotin rabbit polyclonal antibody (ab53494, Abcam, Shanghai, China, 1:200) was used to detect LL37.

Paraffin sections (3 μm) of mouse lungs were processed with xylene, rehydrated with decreasing concentrations of ethanol, and subjected to antigen retrieval in citrate buffer (10 mM, pH 6.0) at 95−100 °C for 15 min. Sections were then incubated with normal rabbit IgG, an anti-Flag tag rabbit monoclonal primary antibody (14793S, Cell Signaling Technology, Shanghai, China, 1:200), and an anti-His tag mouse monoclonal primary antibody (AF5060, Beyotime, 1:200). A Cy3-labeled goat antirabbit secondary antibody (A0516, Beyotime) and an FITC-labeled goat antimouse secondary antibody (A0568, Beyotime) were used to visualize the Flag tag and His tag, respectively. Nuclei were stained with 4′,6-diamidino-2-phenylindole dihydrochloride (DAPI, C1002, Beyotime, Shanghai, China). A Zeiss LSM 780 NLO confocal microscope was employed to visualize the cells.

Western Blot Analysis. A549 and Lewis cells obtained from the Cell Bank of the CAS (Shanghai, China) were seeded into a six-well plate at a density of 1×10^6 cells/well and cultured overnight. S1 (20 μg/mL) preincubated with LL37 (1, 10, and 100 μg/mL) at 37 °C for 15 min was added to the A549 cells, followed by 1 h of coincubation. To evaluate ACE2 cloaking by LL37, cells preincubated with LL37 (10, 50, and 100 μg/mL) for 15 min were exposed to 20 μg/mL S1 for 1 h. After three washes with PBS, the cells were lysed with RIPA lysis and extraction buffer (89900, Thermo Fisher Scientific). An anti-S rabbit polyclonal primary antibody (40591-T62, Sino Biological, 1:1000) and a goat antirabbit secondary antibody (A0208, Beyotime) were employed to detect S1. β-actin was detected with a rabbit monoclonal antibody (AF5003, Beyotime).

Lewis cells were cultured overnight and were then infected with 1×10^8 PFU of adenoviruses expressing Flag-tagged ACE2 (AD-hACE2, Tsingke Biotechnology) at 37 °C for 12 h. A total of 1×10^6 TU of SARS-CoV-2 S pseudovirions expressing His-tagged EGFP (LV-Spike-nCOV, Tsingke Biotechnology) were further added and coincubated at 37 °C for 24 h. After three washes with PBS, the cells were processed for protein extraction. Homogenates of mouse lung

https://doi.org/10.1021/acsinfecdis.1c00096
ACS Infect. Dis. XXXX, XXX, XXX−XXX

samples were prepared using a gentleMACS dissociator (Miltenyi Biotec, Bergisch Gladbach, GER). ACE2, the Flag tag, and the His tag were detected using an anti-ACE2 rabbit polyclonal primary antibody (10108-T24, Sino Biological, 1:1000), the anti-Flag tag rabbit monoclonal primary antibody (1:1000), and the anti-His tag mouse monoclonal primary antibody (1:1000), respectively. A goat antirabbit secondary antibody (A0208, Beyotime), a goat antimouse secondary antibody (A0216, Beyotime), and a BeyoECL Plus chemiluminescence kit (P0018S, Beyotime) were used to visualize the protein bands. This experiment was repeated three times on different days.

MDS. MDS was performed for RBD-LL37 and ACE2-LL37 complexes using molecular docking, molecular dynamics, and structural analysis. Molecular docking was performed on the ZDOCK server (http://zdock.umassmed.edu/) based on the IFACE statistical potential,[51] shape complementarity, and electrostatic potential before the IRaPPA reranking.[52,53] The best docking conformation was selected for MDS. The GROMACS 2020.2 software package, the AMBER99SB-ildn force field, and the TIP3P water model were applied for a total of 500 ns of molecular simulation.[54,55] PyMOL was used to generate images of the biomolecular structures.

Animal Experiment. The animal experiment was approved by the Animal Experimental Ethics Committee of the Third Military Medical University (AMUWEC20201565). Mice were cared for and treated in accordance with the National Institutes of Health (NIH) Guidelines for the Care and Use of Laboratory Animals (NIH publication no. 85e23, rev. 1985). Thirty 8-week-old female C57 mice (18−22 g) were randomly divided into 5 groups (n = 6). Mice were infected with 5×10^8 PFU of adenoviruses (50 μL) and challenged with 2×10^6 TU of SARS-CoV-2 S pseudovirions (30 μL) 5 days later.[33] LL37 treatment (100 μg/mL, 20 μL) was performed after 0.5 h. All viruses and peptides were intranasally administered. To investigate the preventive effect of LL37, the peptide was administered 5 days after adenovirus infection, and the mice were challenged with pseudovirions 0.5 h later. Mice were sacrificed after 24 h to obtain lung samples, which were further analyzed by q-PCR, Western blotting, and immunofluorescence microscopy.

q-PCR. RNA extracted from mouse lungs with TaKaRa (Dalian, Liaoning, China) RNAiso Plus reagent was reverse transcribed using a TaKaRa PrimeScript RT-PCR kit (DRR014A). The primers were as follows: EGFP, 5′-ACGAGTCCAAGTTCTACGGC-3′ (F), 5′-CGGGGATGATCTTCTCGCAG-3′ (R); and β-actin, 5′-TGTACCCAGGCATTGCTGAC-3′ (F), 5′-AACGCAGCTCAGTAACAGTCC-3′ (R). The data were processed with Bio-Rad iQ5 standard edition optical system software (version 2.1). This experiment was conducted in duplicate and repeated three times.

Statistical Analysis. The significance of differences (P) was analyzed with SPSS 25.0 software using one-way ANOVA with the LSD multiple comparison test. A P value of less than 0.05 was defined as statistically significant.

■ ASSOCIATED CONTENT

Supporting Information

The Supporting Information is available free of charge at https://pubs.acs.org/doi/10.1021/acsinfecdis.1c00096.

Sequences, purities, and masses of LL37 and its mutants; additional data showing the inhibition of LL37 on S1 binding to HK-2 cells and its sequence-dependent S1 blocking; results of the pseudovirion infection assay indicating the protection of LL37 pretreatment on HEK-293T-hACE2 cells; and tables showing the molecular interactions between LL37 and RBD and between LL37 and ACE2 (PDF)

■ AUTHOR INFORMATION

Corresponding Authors

Dong-Qing Wei − *AI Research Center, Peng Cheng Laboratory, Shenzhen, Guangdong 518055, China; State Key Laboratory of Microbial Metabolism, Shanghai-Islamabad-Belgrade Joint Innovation Center on Antibacterial Resistances, Joint Laboratory of International Cooperation in Metabolic and Developmental Sciences, Ministry of Education and School of Life Sciences and Biotechnology, Shanghai Jiao Tong University, Shanghai 200030, China;* orcid.org/0000-0003-4200-7502; Email: dqwei@sjtu.edu.cn

Jinghong Zhao − *Department of Nephrology, Xinqiao Hospital, Third Military Medical University, Chongqing 400037, China*; Email: zhaojh@tmmu.edu.cn

Junping Wang − *State Key Laboratory of Trauma, Burns and Combined Injury, Institute of Combined Injury of PLA, Chongqing Engineering Research Center for Nanomedicine, College of Preventive Medicine, Third Military Medical University, Chongqing 400038, China*; Email: wangjunping@tmmu.edu.cn

Authors

Cheng Wang − *State Key Laboratory of Trauma, Burns and Combined Injury, Institute of Combined Injury of PLA, Chongqing Engineering Research Center for Nanomedicine, College of Preventive Medicine, Third Military Medical University, Chongqing 400038, China;* orcid.org/0000-0002-6690-6433

Shaobo Wang − *Department of Nephrology, Xinqiao Hospital, Third Military Medical University, Chongqing 400037, China*

Daixi Li − *Institute of Biothermal Science and Technology, University of Shanghai for Science and Technology, Shanghai 20093, China;* orcid.org/0000-0002-7112-2801

Peiqin Chen − *Institute of Biothermal Science and Technology, University of Shanghai for Science and Technology, Shanghai 20093, China*

Songling Han − *State Key Laboratory of Trauma, Burns and Combined Injury, Institute of Combined Injury of PLA, Chongqing Engineering Research Center for Nanomedicine, College of Preventive Medicine, Third Military Medical University, Chongqing 400038, China*

Gaomei Zhao − *State Key Laboratory of Trauma, Burns and Combined Injury, Institute of Combined Injury of PLA, Chongqing Engineering Research Center for Nanomedicine, College of Preventive Medicine, Third Military Medical University, Chongqing 400038, China*

Yin Chen − *State Key Laboratory of Trauma, Burns and Combined Injury, Institute of Combined Injury of PLA, Chongqing Engineering Research Center for Nanomedicine, College of Preventive Medicine, Third Military Medical University, Chongqing 400038, China*

Jianqi Zhao − *State Key Laboratory of Trauma, Burns and Combined Injury, Institute of Combined Injury of PLA,*

Chongqing Engineering Research Center for Nanomedicine, College of Preventive Medicine, Third Military Medical University, Chongqing 400038, China

Jiachuan Xiong − *Department of Nephrology, Xinqiao Hospital, Third Military Medical University, Chongqing 400037, China*

Jingfei Qiu − *AI Research Center, Peng Cheng Laboratory, Shenzhen, Guangdong 518055, China*

Complete contact information is available at: https://pubs.acs.org/10.1021/acsinfecdis.1c00096

Author Contributions

#C.W., S.W., and D.L. contributed equally to this paper. C.W. performed the binding assay and wrote the paper. S.W. conducted the mouse experiment. D.L. performed the molecular dynamic simulation. P.C. analyzed the computer results. S.H. drew the graphical abstract. G.Z. conducted the q-PCR and analyzed the data. Y.C. performed the Western blot analysis. Jianqi Zhao and J.X. contributed to the pseudovirion infection assay. J.Q. provided the computing resources. D-Q.W., Jinghong Zhao, and J.W. planned the project and edited the paper.

Notes

The authors declare no competing financial interest.

■ ACKNOWLEDGMENTS

This work was supported by the Natural Science Fund of Chongqing City (cstc2019jcyj-msxmX0011), grants from the National Natural Science Foundation of China (nos. 81725019, 32070662, and 61832019), the Program for Scientific and Technological Innovation Leader of Chongqing (CQYC201903084), and Key Research Area Grant 2016YFA0501703 of the Ministry of Science and Technology of China. The computations were performed at the Pengcheng Laboratory.

■ REFERENCES

(1) Coronaviridae Study Group of the International Committee on Taxonomy of Viruses; Gorbalenya, A. E., and Baker, S. C., et al. The Species Severe Acute Respiratory Syndrome-Related Coronavirus: Classifying 2019-nCoV and Naming It SARS-CoV-2. *Nat. Microbiol.* 2020, *5*, 536−544.

(2) Du, L., He, Y., Zhou, Y., Liu, S., Zheng, B., and Jiang, S. (2009) The Spike Protein of SARS-CoV-A Target for Vaccine and Therapeutic Development. *Nat. Rev. Microbiol. 7*, 226−236.

(3) Wrapp, D., Wang, N., Corbett, K. S., Goldsmith, J. A., Hsieh, C. L., Abiona, O., Graham, B. S., and McLellan, J. S. (2020) Cryo-EM Structure of the 2019-nCoV Spike in the Prefusion Conformation. *Science 367*, 1260−1263.

(4) Hoffmann, M., Kleine-Weber, H., Schroeder, S., Krüger, N., Herrler, T., Erichsen, S., Schiergens, T. S., Herrler, G., Wu, N. H., Nitsche, A., Müller, M. A., Drosten, C., and Pöhlmann, S. (2020) SARS-CoV-2 Cell Entry Depends on ACE2 and TMPRSS2 and Is Blocked by a Clinically Proven Protease Inhibitor. *Cell 181*, 271−280.

(5) Shang, J., Wan, Y., Luo, C., Ye, G., Geng, Q., Auerbach, A., and Li, F. (2020) Cell Entry Mechanisms of SARS-CoV-2. *Proc. Natl. Acad. Sci. U. S. A. 117*, 11727−11734.

(6) Matricardi, P. M., Dal Negro, R. W., and Nisini, R. (2020) The First, Holistic Immunological Model of COVID-19: Implications for Prevention, Diagnosis, and Public Health Measures. *Pediatr. Allergy Immunol. 31*, 454−470.

(7) Wang, B., Wang, L., Kong, X., Geng, J., Xiao, D., Ma, C., Jiang, X. M., and Wang, P. H. (2020) Long-Term Coexistence of SARS-CoV-2 with Antibody Response in COVID-19 Patients. *J. Med. Virol. 92*, 1684−1689.

(8) Blanco-Melo, D., Nilsson-Payant, B. E., Liu, W. C., Uhl, S., Hoagland, D., Møller, R., Jordan, T. X., Oishi, K., Panis, M., Sachs, D., Wang, T. T., Schwartz, R. E., Lim, J. K., Albrecht, R. A., and tenOever, B. R. (2020) Imbalanced Host Response to SARS-CoV-2 Drives Development of COVID-19. *Cell 181*, 1036−1045.

(9) Hadjadj, J., Yatim, N., Barnabei, L., Corneau, A., Boussier, J., Smith, N., Péré, H., Charbit, B., Bondet, V., Chenevier-Gobeaux, C., Breillat, P., Carlier, N., Gauzit, R., Morbieu, C., Pène, F., Marin, N., Roche, N., Szwebel, T. A., Merkling, S. H., Treluyer, J. M., Veyer, D., Mouthon, L., Blanc, C., Tharaux, P. L., Rozenberg, F., Fischer, A., Duffy, D., Rieux-Laucat, F., Kernéis, S., and Terrier, B. (2020) Impaired Type I Interferon Activity and Inflammatory Responses in Severe COVID-19 Patients. *Science 369*, 718−724.

(10) Sallard, E., Lescure, F.-X., Yazdanpanah, Y., Mentre, F., and Peiffer-Smadja, N. (2020) Type 1 Interferons as a Potential Treatment against COVID-19. *Antiviral Res. 178*, 104791.

(11) Hancock, R. E. (1997) Peptide Antibiotics. *Lancet 349*, 418−422.

(12) Chen, F., Tang, Y., Zheng, H., Xu, Y., Wang, J., and Wang, C. (2019) Roles of the Conserved Amino Acid Residues in Reduced Human Defensin 5: Cysteine and Arginine Are Indispensable for Its Antibacterial Action and LPS Neutralization. *ChemMedChem 14*, 1457−1465.

(13) Hsu, G. J., Tzang, B. S., Tsai, C. C., Chiu, C. C., Huang, C. Y., and Hsu, T. C. (2011) Effects of Human Parvovirus B19 on Expression of Defensins and Toll-Like Receptors. *Chin. J. Physiol. 54*, 367−376.

(14) Wang, C., Wang, S., Li, D., Wei, D. Q., Zhao, J., and Wang, J. (2020) Human Intestinal Defensin 5 Inhibits SARS-CoV-2 Invasion by Cloaking ACE2. *Gastroenterology 159*, 1145−1147.

(15) Gudmundsson, G. H., Agerberth, B., Odeberg, J., Bergman, T., Olsson, B., and Salcedo, R. (1996) The Human Gene FALL39 and Processing of the Cathelin Precursor to the Antibacterial Peptide LL-37 in Granulocytes. *Eur. J. Biochem. 238*, 325−332.

(16) Laube, D. M., Yim, S., Ryan, L. K., Kisich, K. O., and Diamond, G. (2006) Antimicrobial Peptides in the Airway. *Curr. Top. Microbiol. Immunol. 306*, 153−182.

(17) Wang, C., Wang, S., Chen, Y., Zhao, J., Han, S., Zhao, G., Kang, J., Liu, Y., Wang, L., Wang, X., Xu, Y., Wang, S., Huang, Y., Wang, J., and Zhao, J. Membrane Nanoparticles Derived from ACE2-Rich Cells Block SARS-CoV-2 Infection. *ACS Nano* 2021, DOI: 10.1021/acsnano.0c06836.

(18) Larue, R. C., Xing, E., Kenney, A. D., Zhang, Y., Tuazon, J. A., Li, J., Yount, J. S., Li, P.-K., and Sharma, A. (2021) Rationally Designed ACE2-Derived Peptides Inhibit SARS-CoV-2. *Bioconjugate Chem. 32*, 215−223.

(19) Wan, J., Xing, S., Ding, L., Wang, Y., Gu, C., Wu, Y., Rong, B., Li, C., Wang, S., Chen, K., He, C., Zhu, D., Yuan, S., Qiu, C., Zhao, C., Nie, L., Gao, Z., Jiao, J., Zhang, X., Wang, X., Ying, T., Wang, H., Xie, Y., Lu, Y., Xu, J., and Lan, F. (2020) Human-IgG-Neutralizing Monoclonal Antibodies Block the SARS-CoV-2 Infection. *Cell Rep. 32*, 107918.

(20) Lei, C., Qian, K., Li, T., Zhang, S., Fu, W., Ding, M., and Hu, S. (2020) Neutralization of SARS-CoV-2 Spike Pseudotyped Virus by Recombinant ACE2-Ig. *Nat. Commun. 11*, 2070.

(21) Hamming, I., Timens, W., Bulthuis, M., Lely, A., Navis, G., and van Goor, H. (2004) Tissue Distribution of ACE2 Protein, the Functional Receptor for SARS Coronavirus. A First Step in Understanding SARS Pathogenesis. *J. Pathol. 203*, 631−637.

(22) Du, M., Cai, G., Chen, F., Christiani, D. C., Zhang, Z., and Wang, M. (2020) Multiomics Evaluation of Gastrointestinal and Other Clinical Characteristics of COVID-19. *Gastroenterology 158*, 2298−2301.

(23) Wang, G. (2008) Structures of Human Host Defense Cathelicidin LL-37 and Its Smallest Antimicrobial Peptide KR-12 in Lipid Micelles. *J. Biol. Chem. 283*, 32637−32643.

(24) Jadhav, N. J., Patil, P. S., and Alagarasu, K. (2020) Effect of Full-Length and Truncated Variants of LL-37 on Dengue Virus

Infection and Immunomodulatory Effects of LL-37 in Dengue Virus Infected U937-DC-SIGN Cells. *Int. J. Pept. Res. Ther. 26*, 547−555.
(25) Lan, J., Ge, J., Yu, J., Shan, S., Zhou, H., Fan, S., Zhang, Q., Shi, X., Wang, Q., Zhang, L., and Wang, X. (2020) Structure of the SARS-CoV-2 Spike Receptor-Binding Domain Bound to the ACE2 Receptor. *Nature 581*, 215−220.
(26) Ju, B., Zhang, Q., Ge, J., Wang, R., Sun, J., Ge, X., Yu, J., Shan, S., Zhou, B., Song, S., Tang, X., Yu, J., Lan, J., Yuan, J., Wang, H., Zhao, J., Zhang, S., Wang, Y., Shi, X., Liu, L., Zhao, J., Wang, X., Zhang, Z., and Zhang, L. (2020) Human Neutralizing Antibodies Elicited by SARS-CoV-2 Infection. *Nature 584*, 115−119.
(27) Cao, L., Goreshnik, I., Coventry, B., Case, J. B., Miller, L., Kozodoy, L., Chen, R. E., Carter, L., Walls, A. C., Park, Y. J., Strauch, E. M., Stewart, L., Diamond, M. S., Veesler, D., and Baker, D. (2020) *De Novo* Design of Picomolar SARS-CoV-2 miniprotein Inhibitors. *Science 370*, 426−431.
(28) Melin, A. D., Janiak, M. C., Marrone, F., 3rd, Arora, P. S., and Higham, J. P. (2020) Comparative ACE2 Variation and Primate COVID-19 Risk. *Commun. Biol. 3*, 641.
(29) Vilas Boas, L. C. P., Campos, M. L., Berlanda, R. L. A., de Carvalho Neves, N., and Franco, O. L. (2019) Antiviral Peptides as Promising Therapeutic Drugs. *Cell. Mol. Life Sci. 76*, 3525−3542.
(30) Lou, Z., Sun, Y., and Rao, Z. (2014) Current Progress in Antiviral Strategies. *Trends Pharmacol. Sci. 35*, 86−102.
(31) Klotman, M. E., and Chang, T. L. (2006) Defensins in Innate Antiviral Immunity. *Nat. Rev. Immunol. 6*, 447−456.
(32) Hazrati, E., Galen, B., Lu, W., Wang, W., Ouyang, Y., Keller, M. J., Lehrer, R. I., and Herold, B. C. (2006) Human Alpha- and Beta-Defensins Block Multiple Steps in Herpes Simplex Virus Infection. *J. Immunol. 177*, 8658−8666.
(33) Struck, A. W., Axmann, M., Pfefferle, S., Drosten, C., and Meyer, B. (2012) A Hexapeptide of the Receptor-Binding Domain of SARS Corona Virus Spike Protein Blocks Viral Entry into Host Cells *via* the Human Receptor ACE2. *Antiviral Res. 94*, 288−296.
(34) Arvin, A. M., Fink, K., Schmid, M. A., Cathcart, A., Spreafico, R., Havenar-Daughton, C., Lanzavecchia, A., Corti, D., and Virgin, H. W. (2020) A Perspective on Potential Antibody-Dependent Enhancement of SARS-CoV-2. *Nature 584*, 353−363.
(35) Liu, Q., Fan, C., Li, Q., Zhou, S., Huang, W., Wang, L., Sun, C., Wang, M., Wu, X., Ma, J., Li, B., Xie, L., and Wang, Y. (2017) Antibody-Dependent-Cellular-Cytotoxicity-Inducing Antibodies Significantly Affect the Post-Exposure Treatment of Ebola Virus Infection. *Sci. Rep. 7*, 45552.
(36) Li, Q., Liu, Q., Huang, W., Wu, J., Nie, J., Wang, M., Zhao, C., Zhang, L., and Wang, Y. (2017) An LASV GPC Pseudotyped Virus Based Reporter System Enables Evaluation of Vaccines in Mice under Non-BSL-4 Conditions. *Vaccine 35*, 5172−5178.
(37) Rao, L., Xia, S., Xu, W., Tian, R., Yu, G., Gu, C., Pan, P., Meng, Q. F., Cai, X., Qu, D., Lu, L., Xie, Y., Jiang, S., and Chen, X. (2020) Decoy Nanoparticles Protect against COVID-19 by Concurrently Adsorbing Viruses and Inflammatory Cytokines. *Proc. Natl. Acad. Sci. U. S. A. 117*, 27141−27147.
(38) Vandamme, D., Landuyt, B., Luyten, W., and Schoofs, L. (2012) A Comprehensive Summary of LL-37, the Factotum Human Cathelicidin Peptide. *Cell. Immunol. 280*, 22−35.
(39) Zhu, X., Ge, Y., Wu, T., Zhao, K., Chen, Y., Wu, B., Zhu, F., Zhu, B., and Cui, L. (2020) Co-Infection with Respiratory Pathogens among COVID-2019 Cases. *Virus Res. 285*, 198005.
(40) Scott, A., Weldon, S., Buchanan, P. J., Schock, B., Ernst, R. K., McAuley, D. F., Tunney, M. M., Irwin, C. R., Elborn, J. S., and Taggart, C. C. (2011) Evaluation of the Ability of LL-37 to Neutralise LPS *In Vitro* and *Ex Vivo*. *PLoS One 6*, No. e26525.
(41) Lu, X., Tang, Q., Lindh, M., Dastmalchi, M., Alexanderson, H., Popovic Silwerfeldt, K., Agerberth, B., Lundberg, I. E., and Wick, C. (2017) The Host Defense Peptide LL-37 a Possible Inducer of the Type I Interferon System in Patients with Polymyositis and Dermatomyositis. *J. Autoimmun. 78*, 46−56.
(42) Qin, X., Zhu, G., Huang, L., Zhang, W., Huang, Y., and Xi, X. (2019) LL-37 and Its Analog FF/CAP18 Attenuate Neutrophil Migration in Sepsis-Induced Acute Lung Injury. *J. Cell. Biochem. 120*, 4863−4871.
(43) Liu, P. T., Stenger, S., Li, H., Wenzel, L., Tan, B. H., Krutzik, S. R., Ochoa, M. T., Schauber, J., Wu, K., Meinken, C., Kamen, D. L., Wagner, M., Bals, R., Steinmeyer, A., Zügel, U., Gallo, R. L., Eisenberg, D., Hewison, M., Hollis, B. W., Adams, J. S., Bloom, B. R., and Modlin, R. L. (2006) Toll-Like Receptor Triggering of a Vitamin D-Mediated Human Antimicrobial Response. *Science 311*, 1770−1773.
(44) Peric, M., Koglin, S., Kim, S. M., Morizane, S., Besch, R., Prinz, J. C., Ruzicka, T., Gallo, R. L., and Schauber, J. (2008) IL-17A Enhances Vitamin D3-Induced Expression of Cathelicidin Antimicrobial Peptide in Human Keratinocytes. *J. Immunol. 181*, 8504−8512.
(45) Sørensen, O. E., Follin, P., Johnsen, A. H., Calafat, J., Tjabringa, G. S., Hiemstra, P. S., and Borregaard, N. (2001) Human Cathelicidin, hCAP-18, Is Processed to the Antimicrobial Peptide LL-37 by Extracellular Cleavage with Proteinase 3. *Blood 97*, 3951−3959.
(46) Gombart, A. F., Borregaard, N., and Koeffler, H. P. (2005) Human Cathelicidin Antimicrobial Peptide (CAMP) Gene Is a Direct Target of the Vitamin D Receptor and Is Strongly Up-Regulated in Myeloid Cells by 1,25-Dihydroxyvitamin D3. *FASEB J. 19*, 1067−1077.
(47) D'Avolio, A., Avataneo, V., Manca, A., Cusato, J., De Nicolò, A., Lucchini, R., Keller, F., and Cantù, M. (2020) 25-Hydroxyvitamin D Concentrations Are Lower in Patients with Positive PCR for SARS-CoV-2. *Nutrients 12*, 1359.
(48) Kulkarni, N. N., Yi, Z., Huehnken, C., Agerberth, B., and Gudmundsson, G. H. (2015) Phenylbutyrate Induces Cathelicidin Expression *via* the Vitamin D Receptor: Linkage to Inflammatory and Growth Factor Cytokines Pathways. *Mol. Immunol. 63*, 530−539.
(49) Zumla, A., Hui, D. S., Azhar, E. I., Memish, Z. A., and Maeurer, M. (2020) Reducing Mortality from 2019-nCoV: Host-Directed Therapies Should Be an Option. *Lancet 395*, e35−e36.
(50) Chen, X., Li, R., Pan, Z., Qian, C., Yang, Y., You, R., Zhao, J., Liu, P., Gao, L., Li, Z., Huang, Q., Xu, L., Tang, J., Tian, Q., Yao, W., Hu, L., Yan, X., Zhou, X., Wu, Y., Deng, K., Zhang, Z., Qian, Z., Chen, Y., and Ye, L. (2020) Human Monoclonal Antibodies Block the Binding of SARS-CoV-2 Spike Protein to Angiotensin Converting Enzyme 2 Receptor. *Cell. Mol. Immunol. 17*, 647−649.
(51) Pierce, B. G., Wiehe, K., Hwang, H., Kim, B. H., Vreven, T., and Weng, Z. (2014) ZDOCK Server: Interactive Docking Prediction of Protein-Protein Complexes and Symmetric Multimers. *Bioinformatics 30*, 1771−1773.
(52) Pierce, B. G., Hourai, Y., and Weng, Z. (2011) Accelerating Protein Docking in ZDOCK Using an Advanced 3D Convolution Library. *PLoS One 6*, No. e24657.
(53) Mintseris, J., Pierce, B., Wiehe, K., Anderson, R., Chen, R., and Weng, Z. (2007) Integrating Statistical Pair Potentials into Protein Complex Prediction. *Proteins: Struct., Funct., Genet. 69*, 511−520.
(54) Rakhshani, H., Dehghanian, E., and Rahati, A. (2019) Enhanced GROMACS: Toward a Better Numerical Simulation Framework. *J. Mol. Model. 25*, 355.
(55) Pang, Y. P. (2016) FF12MC: A Revised AMBER Forcefield and New Protein Simulation Protocol. *Proteins: Struct., Funct., Genet. 84*, 1490−1516.

https://doi.org/10.1021/acsinfecdis.1c00096
ACS Infect. Dis. XXXX, XXX, XXX−XXX